Estuarine, Coastal and Shelf Science 133 (2013) 129–136

Contents lists available at ScienceDirect

Estuarine, Coastal and Shelf Science

journal homepage: www.elsevier.com/locate/ecss

The significance of ultra-refracted surface gravity waves on sheltered coasts, with application to San Francisco Bay

D.M. Hanes [a,*], L.H. Erikson [b]

[a] Earth and Atmospheric Sciences, Saint Louis University, 3642 Lindell Blvd., Saint Louis, MO 63108, United States
[b] U.S.G.S. Coastal and Marine Geology Program, United States

ARTICLE INFO

Article history:
Received 7 June 2013
Accepted 15 August 2013
Available online 29 August 2013

Keywords:
ocean waves
coastal processes
refraction

ABSTRACT

Ocean surface gravity waves propagating over shallow bathymetry undergo spatial modification of propagation direction and energy density, commonly due to refraction and shoaling. If the bathymetric variations are significant the waves can undergo changes in their direction of propagation (relative to deepwater) greater than 90° over relatively short spatial scales. We refer to this phenomenon as ultra-refraction. Ultra-refracted swell waves can have a powerful influence on coastal areas that otherwise appear to be sheltered from ocean waves. Through a numerical modeling investigation it is shown that San Francisco Bay, one of the earth's largest and most protected natural harbors, is vulnerable to ultra-refracted ocean waves, particularly southwest incident swell. The flux of wave energy into San Francisco Bay results from wave transformation due to the bathymetry and orientation of the large ebb tidal delta, and deep, narrow channel through the Golden Gate. For example, ultra-refracted swell waves play a critical role in the intermittent closure of the entrance to Crissy Field Marsh, a small restored tidal wetland located on the sheltered north-facing coast approximately 1.5 km east of the Golden Gate Bridge.

1. Introduction

It is well known that surface gravity waves undergo transformation when the water depth is less than approximately their wavelength. Depending on the severity of the bathymetry and its spatial gradient, phenomenon such as wave refraction, shoaling, reflection, diffraction, and dissipation may occur. In particular, the directions of wave and energy propagation can be drastically modified, mainly through refraction although the other phenomenon mentioned above can also contribute. For example, wave theory explains that when idealized single frequency waves approaching an isolated island from the deep ocean, the waves can actually impact the shoreline on the lee side of the island, having undergone a nearly 180° change in the direction of wave propagation (e.g. Lautenbacher, 1970; Jonsson et al., 1976; Liu et al., 1995). We will refer to surface gravity waves that have undergone a 90° or more directional change from their deepwater propagation direction as Ultra-Refracted Waves (URW). Because of the manner in which wave direction changes in response to bathymetry, URW can propagate into areas that appear to be sheltered from ocean waves, such as the lee side of islands, into coastal lagoons, bays, and estuaries, and onto coastlines protected by large scale cusps and promontories.

San Francisco Bay (see Fig. 1A) is one of the largest and most sheltered natural harbors on earth. The bay is normally protected from ocean waves by the coastal orientation, the offshore bathymetry, and the narrow entrance at the Golden Gate (hereafter referred to as GG). In fact, refraction and breaking of storm waves over the large ebb tidal delta plays a significant role in driving coastal processes near the mouth of San Francisco Bay (Eshleman et al., 2007; Shi et al., 2011). However, wave refraction (and other less significant processes) can also cause deep water ocean swell waves to enter through the GG straight and spread throughout central San Francisco Bay. The ocean waves that propagate through the GG can exert strong influence on coastal processes and ecology within the Bay (e.g., Talke and Stacey, 2003).

The present work utilizes a widely used numerical model for wave propagation to explore the degree to which URW penetrate through the GG straight and into San Francisco Bay. The role of wave frequency and deep water direction are explored through a series of model runs. Transects were created in the model at four locations, as shown in Fig. 1B, and the wave energy for various wave cases were evaluated on these transects. A sequence of simulations was conducted to explore the influence of deep water wave characteristics such as frequency, height, and direction.

* Corresponding author.
E-mail address: dhanes@slu.edu (D.M. Hanes).

0272-7714/$ – see front matter © 2013 Elsevier Ltd. All rights reserved.
http://dx.doi.org/10.1016/j.ecss.2013.08.022

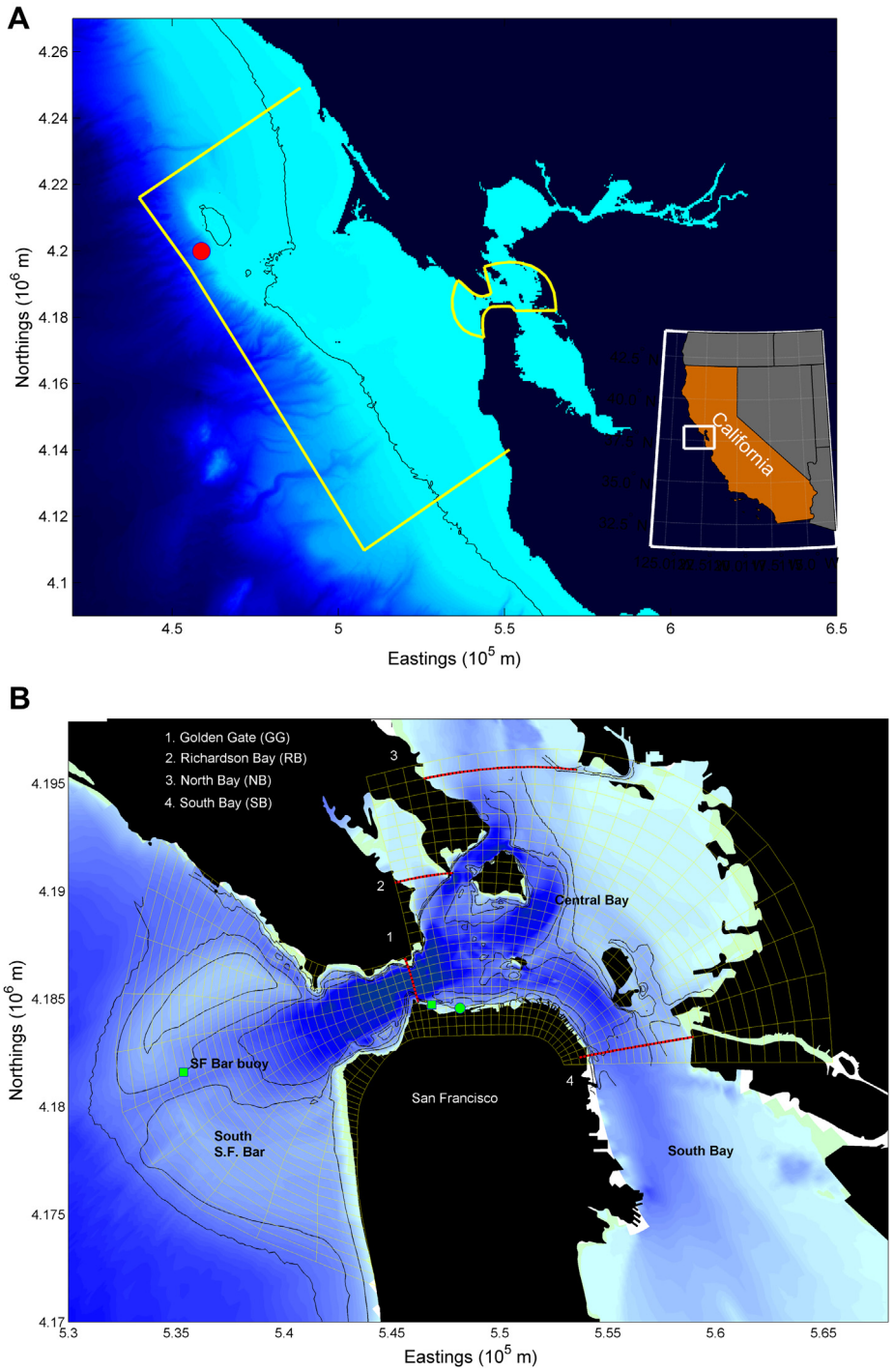

Fig. 1. A: Study area and model grids. Outlines of the two curvilinear grids used in the numerical are shown with solid yellow lines. Black lines are the 100 m isobaths. The red circle denotes location of the deep-water Pt. Reyes wave buoy. B: San Francisco Central Bay study area. Nested model grid (de-refined) is shown as light-colored hatching; red/black lines indicate transects discussed in text. Wave measurement locations: SF Bar wave buoy (green square), CF1 (green square) and CF2 (green circle) near shore Crissy Field shoreline. Contours are the 10, 15, and 20 m isobaths. (For interpretation of the references to color in this figure legend, the reader is referred to the web version of this article.)

2. Wave model

The spectral wave model SWAN (Booij et al., 1999; Ris et al., 1999) was used to simulate wave propagation from deep water. The model has been used widely in the coastal engineering and science community, and for this study was implemented through the Deltares Delft3D user interface (version 3.28.04, SWAN version 40.51). The SWAN model is a phase averaged numerical model capable of simulating wave refraction and shoaling owing to bathymetry, wave–current interaction, non-linear wave–wave energy transfers, and energy dissipation from white-capping, depth-induced wave breaking, and bottom shear stress. Evolution of the wave spectrum in SWAN is described by the spectral action balance equation, which in Cartesian coordinates may be expressed as,

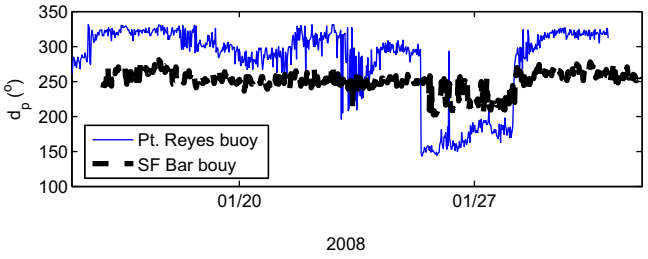

Fig. 2. Wave angle measured at the offshore Pt. Reyes Buoy and S.F. Bar buoy.

$$\frac{\partial}{\partial t}N+\frac{\partial}{\partial x}C_xN+\frac{\partial}{\partial y}C_yN+\frac{\partial}{\partial f}C_fN+\frac{\partial}{\partial \theta}C_\theta N=\frac{S}{f} \quad (1)$$

where N is the wave action density, t, x, and y are space and time coordinates, respectively, f is the frequency, θ is the direction, and S is a source term representing the effects of generation, dissipation and nonlinear wave–wave interactions. Wave energy dissipation due to bottom friction was assumed to be related to a semi-empirical expression derived from the Jonswap spectrum with the coefficient for swell conditions = 0.038 $m^2\ s^{-3}$ (Hasselmann et al., 1973). Depth-induced breaking followed that of the Battjes and Stive (1985) model. In the simulations performed for this study, non-linear wave–wave interactions as well as diffraction and current–wave interactions were notably not accounted for, even though they probably occur at some times and to some extent, and it is recognized that the model only approximately describes the actual physics of wave propagation and transformation. Neglecting diffraction, wave–current interactions, and non-linear wave–wave interactions is justified in the present work by the result that the model accurately describes most of the measured changes in wave direction. As a follow-up to this study it would be useful to improve accuracy to model spectral wave diffraction as well as refraction, such as suggested by Holthuijsen et al. (2003).

2.1. Bathymetry and model grids

Offshore bathymetry for the regional grid was obtained from NOAA (70 m–200 m resolution). Bathymetry across the delta, through the GG, and in Central Bay utilized high-resolution multi-beam measurements obtained by the seafloor mapping lab at California State University, Monterey in 2005 and 2008 (http://seafloor.csumb.edu/SFMLwebDATA_SURVEYMAP.htm). Nearshore bathymetry from the GG to San Francisco Marina about 1100 m east of Crissy Marsh inlet was measured in January 2008 using single-beam transducers and real time kinematic global positioning system along cross- and along-shore transects. Bathymetry across the continental shelf to the GG inlet is complicated by the presence of the Farallon Islands (located about 40 km west of the GG), the large ebb tidal delta, and the GG Strait. Bathymetry just inside the Gate is complicated by the presence of a hard-rock promontory and very steep lateral bed slopes on the sides of the GG Straight. These bathymetric variations across the continental shelf from the model boundary to the southern shores of San Francisco's Central Bay cause significant wave refraction and shoaling, and sometimes result in URWs.

Model grids consisted of an outer regional grid (Fig. 1A) extending from beyond the continental shelf in 1000 m water depth more than 80 km offshore of the GG, and a smaller nested grid. The outer regional grid consists of three open boundaries, with a grid cell size of approximately 1 km × 1 km. The higher resolution of the nested grid, covering Central Bay and GG inlet (Fig. 1B), is approximately 30 by 40 m.

2.2. Model validation

Even though the SWAN model has been calibrated and validated in numerous locations worldwide, because of the unusual bathymetry in the San Francisco region it is prudent to validate the model capabilities in predicting the arrival of ocean waves inside the entrance to San Francisco Bay. Wave measuring instrumentation (1 MHz Nortek AWAC) was deployed near the Crissy Field Marsh shoreline in January, 2008 at 4 m and 3 m water depths at sites CF1 and CF2, respectively. Model input was provided by the California Data Information Program (CDIP) Pt. Reyes buoy (Station # 029) in a water depth of 550 m (see Fig. 1A). Spectral measurements obtained by the California Data Information Program (CDIP) at the S.F. Bar buoy (Station # 142) in approximately 20 m water depth were also used for comparison with model predictions. Waves in this region typically consist of swell waves generated

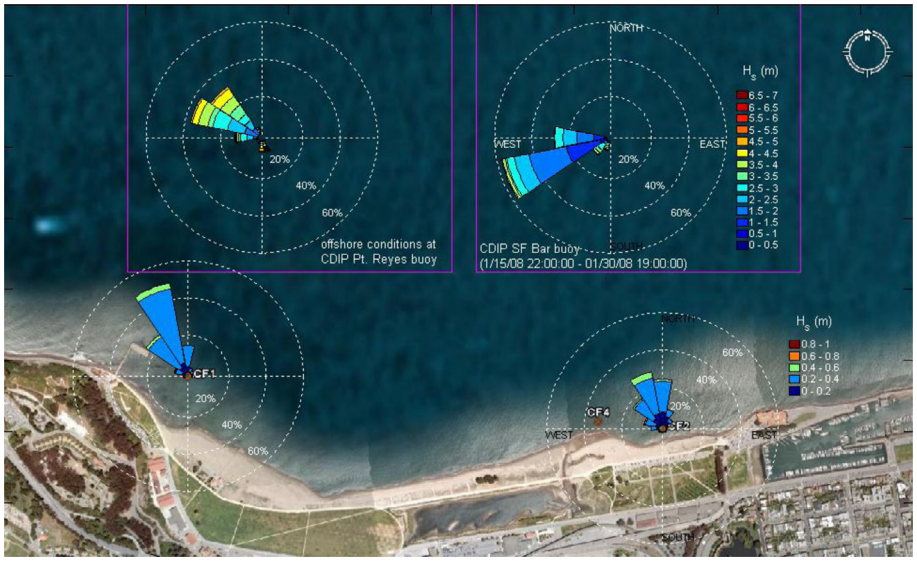

Fig. 3. Wave roses in deep water, on the S.F. Bar, and near the Crissy Field shoreline for January 2008 indicate large variability in wave direction.

(anywhere) in the Pacific Ocean with periods ranging from 8 s to 18 s, and locally generated wind waves with periods less than 10 s. We will use the term "swell waves" to indicate waves with periods of 10 s or greater.

Measured peak wave directions (d_p), that is, the directional sector with the highest wave energy, at the SF Bar buoy and the offshore Pt. Reyes buoy are shown in Fig. 2 for times corresponding to the CF1 and CF2 measurements (January 14–28, 2008). The convention used for direction is the angle from which the waves are propagating, with 0/360° being true north, and clockwise positive directions. Peak directions observed at the offshore CDIP Pt. Reyes buoy indicate that swell came predominantly from the northwest (~300°), with a southwest swell event ($150° < d_p < 200°$) that lasted several days centered around 27 Jan 2008. The wave angles measured at the S.F. Bar buoy are substantially different from the offshore wave angles, indicating that strong refraction occurs over the shelf and ebb tidal delta, shifting the wave direction angle by approximately 50° toward a more westerly approach. The wave directions at the shallow CF1 and CF2 sites, as well as the deeper sites, are shown in Fig. 3. The wave direction clearly undergoes radical changes as the waves propagate from deep water over the complex bathymetry of the S.F. Bar, and to the shoreline of Crissy Field.

For purposes of model validation, the model results are compared to measured waves in Fig. 4, which shows the correlations between modeled and measured waves as a function of wave frequency. Because the model was forced with offshore deep-water spectral wave measurements, energy from local wind-generated waves are not included in the simulations. The modeled and measured wave characteristics are therefore best compared in the frequency domain. Correlation coefficients were computed between time-series of hourly model and observation 1D spectra (Jan 16–26 2008). This was done by computing the total energy (from all directions) in 0.33 Hz (3 s) bins (moving window discretized at 0.5 s from 1 s to 30 s) for each hourly time step. This resulted in time-series representations of modeled and observed energy at each frequency bin, for correlation coefficients were then computed and plotted against frequency in Fig. 4. The correlations between model predictions and measurements for swell periods ($f < 0.083$ Hz, $t_p > 12$ s) range between 0.4 and 0.8. Correlations decrease significantly (as expected) for local wind-generated frequencies ($f > 0.167$ Hz, $t_p < 6$ s). Overall the agreement between the model and the measurements was quite good for both the S.F. bar buoy site in 20 m depth and the Crissy Marsh sites in approximately 3 m water depth inside the entrance to S.F. Bay. These validation results provide evidence that the simple spectral model employed to predict wave transformation is adequate to capture most of the changes in the waves.

3. Numerical experiments and results

A series of simulations was conducted to estimate the propagation of deep water ocean waves to the Golden Gate (GG) entrance and further into San Francisco Bay. Offshore wave directions were discretized into six direction sectors (d_p = 165°, 195°, 225°, 255°, 285°, and 315°), with peak periods from 10 s to 18 s at 1 s intervals, and significant wave heights equal to 2 m and 5 m, giving a total of 108 simulations. Boundary input 2D spectra were defined with the JONSWAP spectrum. The spectra were described with a peak enhancement factor = 3.3, 36 direction bins ($\Delta\theta = 10°$), and 35 frequencies with logarithmic spacing from 0.05 to 1.0 Hz. The ratio of the model predicted energy flux at the GG was compared to the deep water input energy flux, for each of six deep water directional sectors. The ratio of deep water energy flux to energy flux at the GG will be referred to as the RE (relative energy).

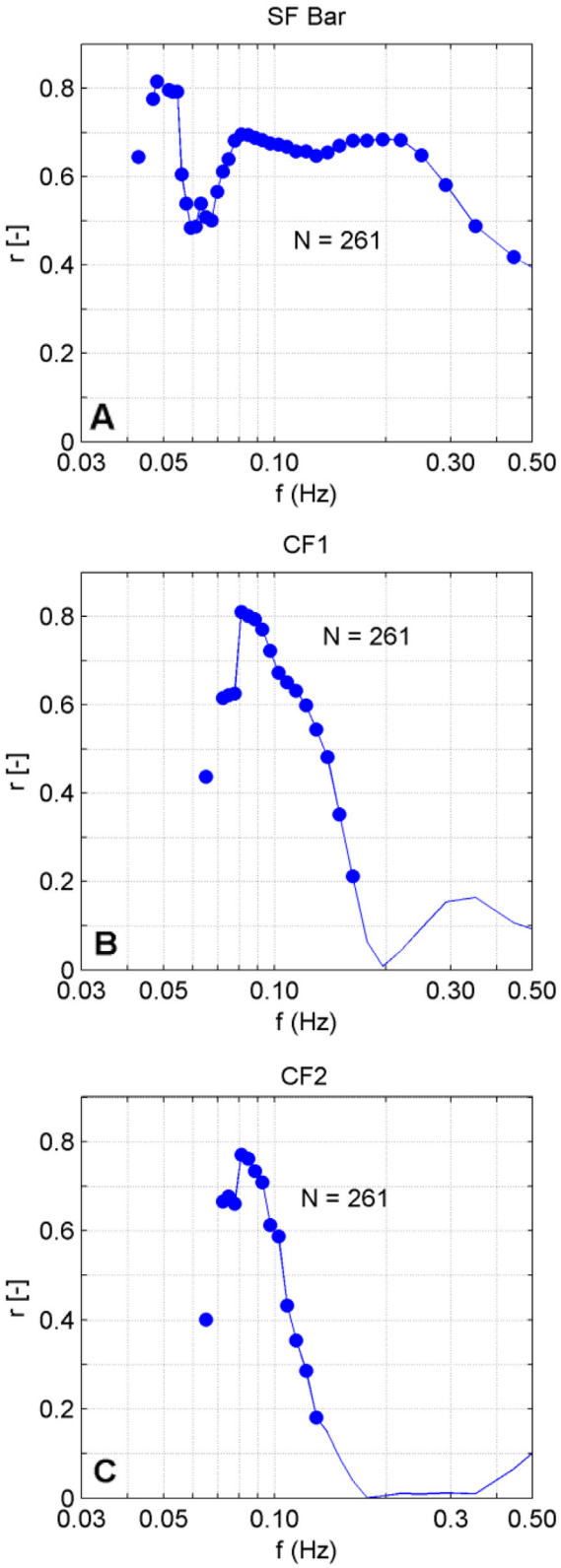

Fig. 4. Correlations between measured and modeled wave energy as a function of frequency at the CDIP S.F. Bar bouy (top), CF1 (middle), and CF2 (bottom) sites. Points that are statistically significant (p-value < 0.005) are shown with filled circles.

For each simulation the wave energy flux (EF) perpendicular to each grid cell (denoted by subscript i) along the transects of GG, Richardson Bay (RB), North Bay (NB), and South Bay (SB) (see Fig. 1B) were computed as follows:

$$EF_i = \int \rho g C_i(f) E_i(f) \mathrm{d}f \quad (2)$$

where $E_i(f)$ is the energy density spectrum in units of m^2/hz, $C_i(f)$ is the component of the group velocity (m/s) perpendicular to the transect at the center of each grid cell, ρ = water density (1025 kg/m^3), and g = gravitational acceleration (9.81 m/s^2). Wave energy flux was then summed using the weighted grid cell length along each transect to compute the spatially averaged energy flux through the transect:

$$\overline{EF} = \sum_{i=1}^{N} EF_i(\Delta x_i / X) \quad (3)$$

where EF_i = energy flux at the center point of cell i given by Equation (2), Δx_i is the along-transect length of grid cell i, and, X is the total length of the transect.

$\overline{EF}$ at the GG ranges from approximately 2–21% of the deepwater energy flux depending upon wave conditions (Figs. 5 and 6). The decrease in energy flux between deep water and the GG is mainly due to refraction of waves away from the GG and toward the adjacent coast, and the dissipation of large waves over the ebb tidal delta. For any given deep water wave period there is a peak in the RE at the GG corresponding to a deep water direction from the southwest. The peak is most pronounced for the short (t_p = 6 s) period waves, with maximum RE at the GG corresponding to a deep water direction from 240°. For longer period waves the deep water direction resulting in the highest RE at the GG shifts slightly southward, while the directional dependence decreases significantly. Peak RE at the GG occurred with offshore incidence angles between 200° and 250° in all cases. The extremes of 195° and 315° both show the least RE.

The smaller RE from waves originating in the west and northwest is due to the geographical layout of the landmasses and orientation of the GG, as well as the shadowing effect of the Farallon Islands, located approximately 40 km west of the GG. The orientation of the GG inlet and shipping channel is 245° which, if lacking complex bathymetry, would suggest that RE from this direction would be greatest. However, model results suggests that the RE making to the GG from more southerly directions can be even greater, even for long period ocean swell waves. There is significant dissipation of wave energy across the northern lobe of the ebb tidal delta (often referred to as the San Francisco Bar or "potato patch"). Water depths across the northern lobe of the delta (min depth ~8 m) are about 30% shallower than the southern lobe (min depth ~ 11 m) enabling greater dissipation in addition to greater shoaling and refraction. For the case of the 2 m incident wave from the 210°–240° direction, the model predicts energy dissipation across the northern lobe (max dissipation ~3.3 N/m^2) to be more than twice as much compared to energy dissipation across the southern lobe (max dissipation ~1.5 N/m^2).

RE at the GG is greater for shorter waves in comparison to longer waves, because the shorter waves refract toward the outer adjacent coast less than the longer waves. While this is the case for both the 2 m and 5 m wave cases simulated, the relative amount of energy that makes it through the GG is decreased for the higher wave condition. The decreased RE is due to the greater percent of breaking waves over the shoals as well increased offshore energy flux (Eq. (3)) in the denominator of RE.

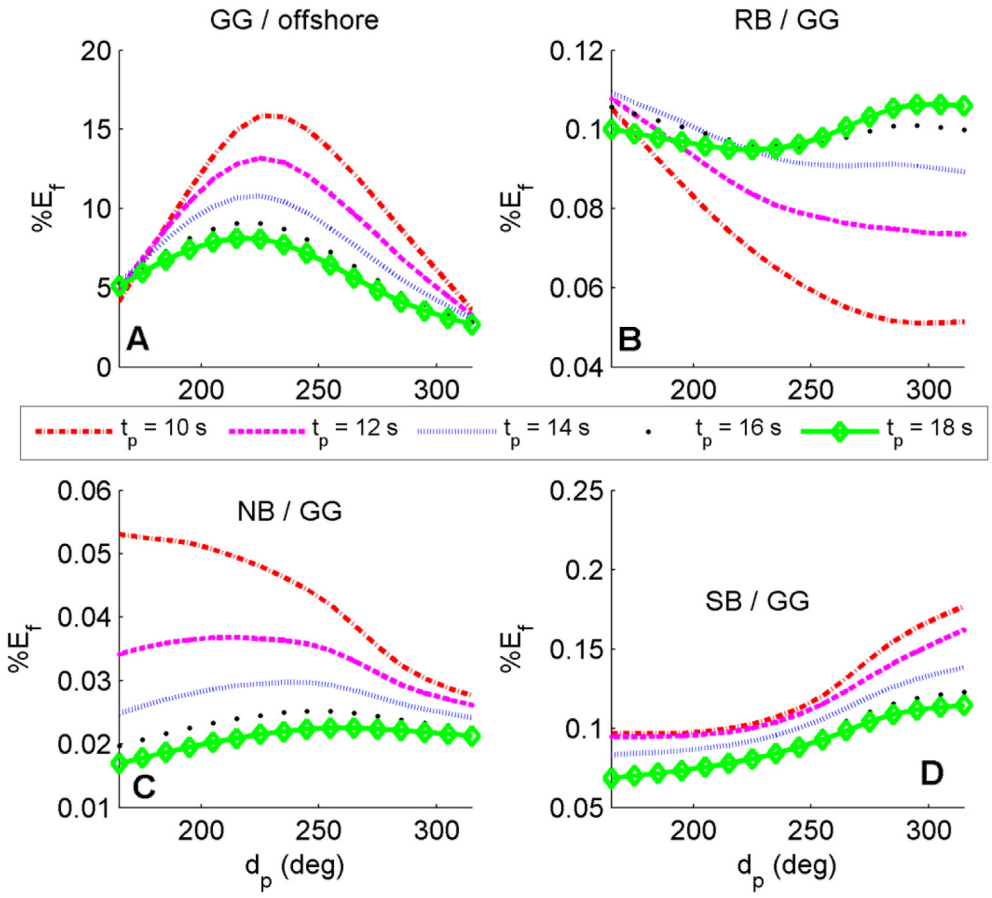

Fig. 5. Relative energy in relation to offshore deepwater wave direction for h_s = 2 m and t_p from 6 to 22 s at 2 s increments. Total energy across (A) Golden Gate inlet normalized by offshore wave energy and across Richardson Bay (RB), North Bay (NB), and South Bay (SB) transects all normalized by total energy at Golden Gate.

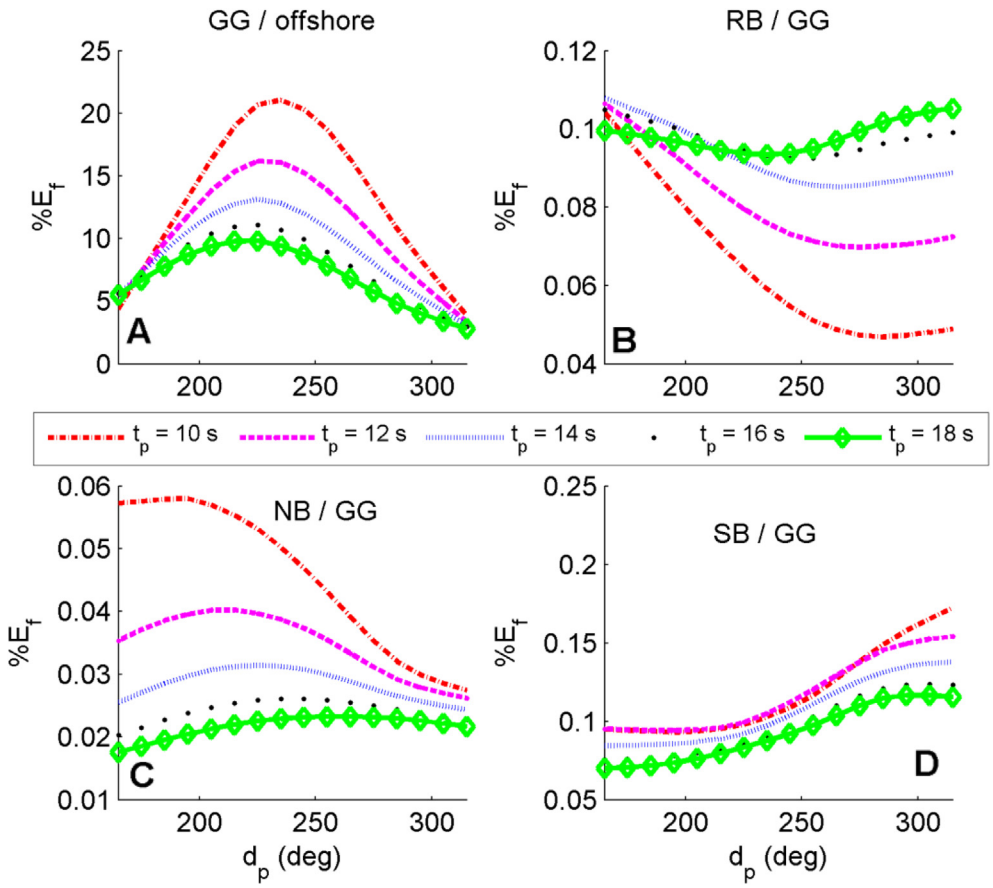

Fig. 6. Relative energy in relation to offshore deepwater wave direction for $h_s = 5$ m and t_p from 6 to 22 s at 2 s increments. Total energy across (A) Golden Gate inlet normalized by offshore wave energy and across Richardson Bay (RB), North Bay (NB), and South Bay (SB) transects all normalized by total energy at Golden Gate.

Waves that enter through the GG may propagate into Richardson Bay (RB, the small bay immediately to the North of the GG), northern San Francisco Bay (NB), or southern San Francisco Bay (SB). The wave energy flux along transects at the entrances to RB, NB, and SB are compared to the wave energy flux at the GG in Figs. 5 and 6, for offshore wave heights of 2 m and 5 m, respectively. Only a small fraction (<1%) of the energy flux through the GG makes it into these bays, and the amount depends upon deep water frequency and direction. RB is most vulnerable to longer period swell, NB is more vulnerable to shorter period waves, and SB is vulnerable to all swell waves, particularly those coming from the north in deep water. But overall, the vast majority of the wave energy that enters through the GG is dissipated in central San Francisco Bay.

3.1. Application to Crissy Field Marsh

Since its restoration as a tidal wetland in the late 1990's the entrance to Crissy Field Marsh has closed on at least 46 occasions. Battalio et al. (2006) and Hanes et al. (2011) show that the times of closure tend to occur at times with large offshore ocean waves typically originating in the north pacific ocean. Hanes et al. (2011) also identifies a few closure events that occurred with relatively low offshore waves, and suggested based on the deep water wave directional spectrum, swell waves from the southern hemisphere might be responsible for the marsh entrance closure during these times. For example, the deep-water wave spectra for two particular times with relatively small wave energy, but when the entrance to Crissy Field Marsh closed, are shown in Fig. 7. The upper panel is from 09:28 h, 9/3/2003 UTC, when the deep-water significant wave height was 1.66 m, and the lower panel is from 22:07 h, 6/1/2010 UTC, when the deep-water significant wave height was 2.03 m. For comparison, the average deep water significant wave height at this location is approximately 2.5 m, so these examples represent time periods with relatively low wave heights. Both spectra indicate the main peak in wave energy is from the northwest, as is typical, but an unusual secondary peak in low frequency swell is coming from the southwest. The present work helps explain how the relatively small wave energy coming from the south will refract toward Crissy Marsh and subsequently influence littoral processes at the marsh entrance.

The majority of the swell energy passing through the Golden Gate becomes aligned with the deepest part of the inlet and is directed toward the central part of the Bay where it dissipates as it propagates and over the shallow portions at the east end. At the eastern end of the Golden Gate inlet, swell energy that has propagated along the channel undergoes a radical change in direction due to refraction over the complex and very steep bathymetry. These ultra-refracted waves result in a focusing of swell energy at the north facing coastline of Crissy Marsh, as shown previously by the wave roses in Fig. 3. The skewed incidence angle of ocean swells along Crissy Beach causes eastward directed long-shore sediment transport, which is likely the cause for sand accumulation and intermittent closure of the Crissy Field Marsh inlet.

These results can be summarized by examining the wave energy flux arriving at the Crissy Field shoreline relative to the wave energy flux in deep water, as a function of deep water wave direction. The size of the arrows in Fig. 8 indicate this relative ratio for the six sectors of deep water wave direction, where the white arrows indicate peak wave periods between 6 s and 12 s, and the gray

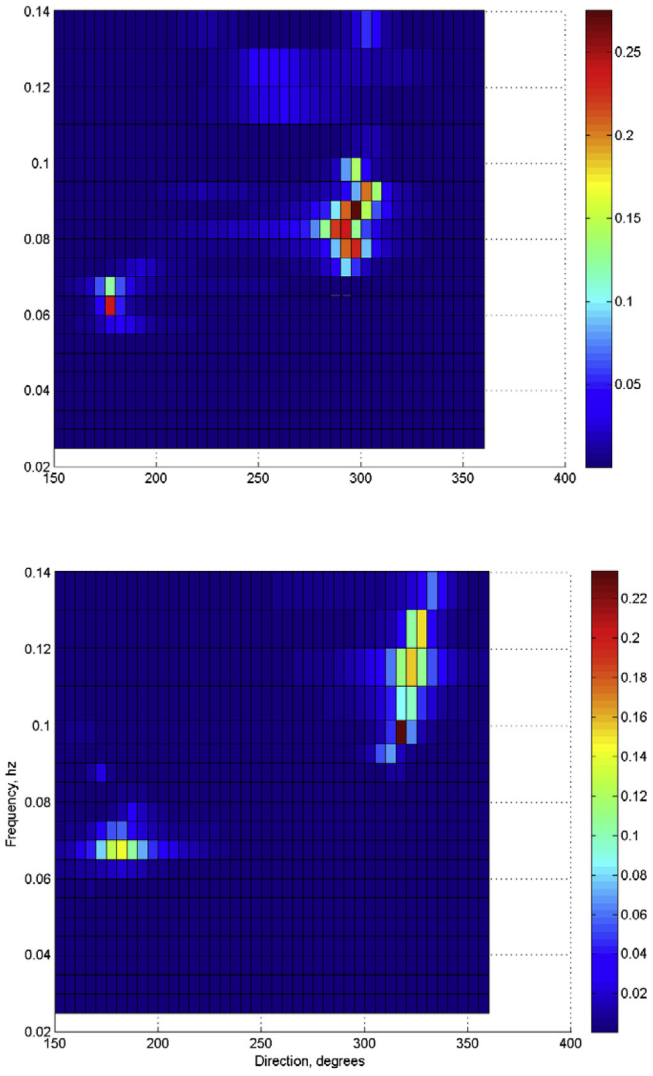

Fig. 7. Deep water directional wave spectra on 9/3/2003 09:28 h UTC (upper) and 6/1/2010 22:07hr UTC (lower), when the entrance to CFM closed. Units are m^2/Hz/deg.

arrows indicate peak wave periods between 12 s and 18 s. The numerical values outside the circle simply indicate the ranking of the relative wave energies. Clearly the greatest amount of relative deep water energy reaching the Crissy Field shoreline comes from the southwest, even though the shoreline faces north.

It is worth noting that swell waves propagating to this region from their origin in the southern hemisphere typically undergo weak non-linear interactions that leads to significant groupiness (Elgar et al., 1984), and nonlinear skewed waves in shallow water (Elfrink et al., 2006). It is well known that both wave groups (e.g. Vincent and Hanes, 2002; Dohmen-Janssen and Hanes, 2005) and wave skewness (e.g. Yu et al., 2010) can enhance sediment transport. This is another factor that could lead to relatively small waves arriving from the southern hemisphere having an impact on sediment dynamics that would be more typical of larger waves.

4. Conclusions

The results of the wave propagation simulations indicate that deep water propagation from the southwest results in more relative energy penetration through the GG, and reaching the Crissy Field shoreline, than from other directions. In reality, waves originating from the southwest are typically long swell waves generated by large

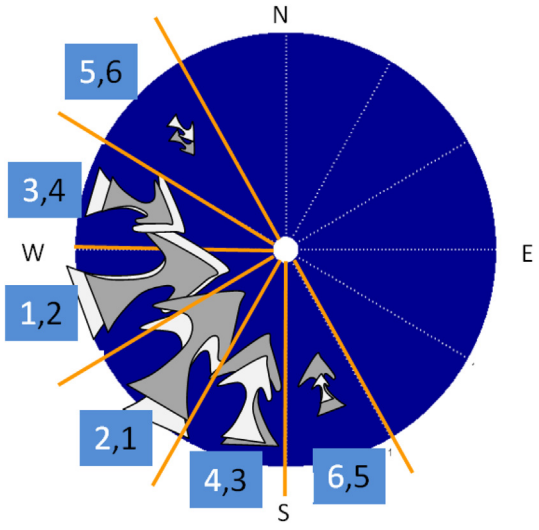

Fig. 8. Conceptual diagram of relative energy flux at the Crissy Field shoreline compared to offshore deep-water energy flux for intermediate (6 s $\leq t_p \leq$ 12 s; white arrows) and long-period waves ($t_p >$ 12 s; gray arrows). Arrows are scaled relative to the maximum RE of intermediate period waves from the SW (210°–240°). White and black numbers denote ranking of greatest to smallest RE of intermediate- and long-period waves, respectively.

storms in the southern hemisphere. While the deep water southwest incident waves result in more RE through GG compared to other incidence angles, the occurrence of these conditions are relatively rare (Fig. 9). The simulations also indicate that there exists a threshold input wave energy (between 2 m and 5 m) such that larger offshore waves dissipate more energy over the ebb tidal delta due to wave breaking, resulting in lower energy reaching the bay.

Talke and Stacey (2003) measured near-bed velocity and sediment concentrations at the east end of Central Bay and noted that during periods when tidal forcing was limited and wind waves were small, remotely forced ocean swells were an important energy source of near-bed energy and shear stress on estuarine mudflats. The model results presented in this study are consistent with their statements and raise the possibility that most of the mudflats within Central Bay could be affected by ocean swell. Although not addressed in this study, the effect is likely to be even greater during

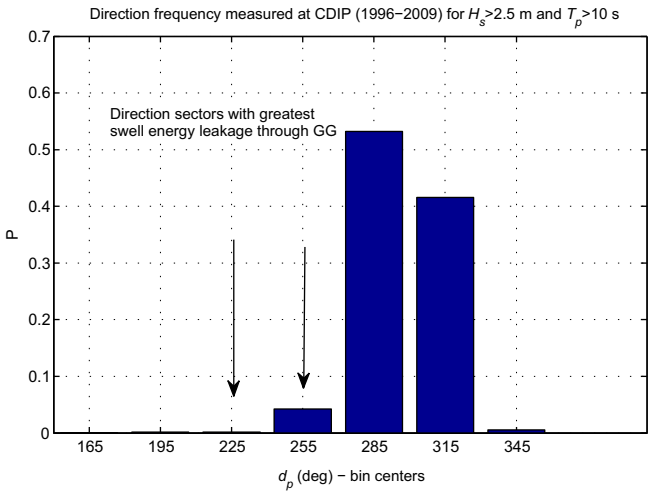

Fig. 9. Deep water wave histogram measured at CDIP Pt. Reyes buoy (1996–2009) for $h_s \geq$ 2.5 m and $t_p >$ 10 s. Most common deep-water wave direction is from the northwest at 285° and 315°.

flood events when strong tidal currents and high tides enable a greater transfer of energy through the GG.

Finally it should be mentioned that wave diffraction, wave reflection, and wave–current interaction, which were not considered here, probably play a significant role in transforming waves upon their approach to San Francisco Bay, and distributing wave energy throughout the bay once it enters through the golden gate.

Acknowledgments

The initial portions of this work were supported by the Coastal and Marine Geology Program of the U.S. Geological Survey. For the latter portion of the work DMH was support by Saint Louis University. The authors appreciate the assistance provided by Edwin Elias, Patrick Barnard, Jeff Hansen, and the USGS Marine Facilities group, the helpful reviews provided by two anonymous reviewers, and the very thorough and helpful review of Ruben Kos'yan.

References

Battalio, B., Danmeier, D., Williams, P., 2006. Predicting closure and breaching frequencies of small tidal inlets—a quantified conceptual model. In: Proceedings of the International Conference on Coastal Engineering, San Diego.

Battjes, J.A., Stive, M.J.F., 1985. Calibration and verification of a dissipation model for random breaking waves. Journal of Geophysical Research-Oceans 90 (NC5), 9159–9167.

Booij, N., Ris, R.C., Holthuijsen, L.H., 1999. A third-generation wave model for coastal regions. Part 1, model description and validation. Journal of Geophysical Research 104 (C4), 7649–7666.

Dohmen-Janssen, C.M., Hanes, D.M., 2005. Sheet flow and suspension under wave groups in a large wave flume. Continental Shelf Research 25, 333–347.

Elfrink, B., Hanes, D.M., Ruessink, G.B., 2006. Parameterization and simulation of near bed orbital velocities under irregular waves in shallow water. Coastal Engineering 53 (11), 915–927.

Elgar, S., Guza, R.T., Seymour, R.J., 1984. Groups of waves in shallow water. Journal of Geophysical Research-Oceans 89 (NC3), 3623–3634.

Eshleman, J.L., Barnard, P.L., Erikson, L.H., Hanes, D.M., 2007. Coupling alongshore variations in wave energy to beach morphologic change using the SWAN wave model at Ocean Beach, San Francisco, CA. In: 10th International Workshop on Wave Hindcasting and Forecasting, Oahu, Hawaii, November 11–16, 2007, p. 20. Paper F4.

Hanes, D.M., Ward, K., Erikson, L.H., 2011. Waves and tides responsible for the intermittent closure of the entrance to a small, sheltered tidal wetland at San Francisco, California. Continental Shelf Research. http://dx.doi.org/10.1016/j.csr.2011.07.004.

Hasselmann, K., Barnett, T.P., Bouws, E., Carlson, H., Cartwright, D.E., Enke, K., Ewing, J., Gienapp, H., Hasselmann, D.E., Kruseman, P., Meerburg, A., Müller, P., Olbers, D.J., Richter, K., Sell, W., Walden, H., 1973. Measurements of wind wave growth and swell decay during the Joint North Sea Wave Project (JONSWAP). Deutsche Hydrographische Zeitschrift 8 (12).

Holthuijsen, L.H., Herman, A., Booij, N., 2003. Phase-decoupled refraction-diffraction for spectral wave models. Coastal Engineering 49 (4), 291–305.

Jonsson, I.G., Skovgaard, O., Brinkkjaer, O., 1976. Diffraction and refraction calculations for waves incident on an island. Journal of Marine Research 34, 469–496.

Lautenbacher, C.C., 1970. Gravity wave refraction by islands. Journal of Fluid Mechanics 41 (655).

Liu, P.L.F., Cho, Y.S., Briggs, M.J., et al., 1995. Runup of solitary waves on a circular island. Journal of Fluid Mechanics 302, 259–285.

Ris, R.C., Holthuijsen, L.H., Booij, N., 1999. A third-generation wave model for coastal regions. Part 2, model description and validation. Journal of Geophysical Research 104 (C4), 7649–7666.

Shi, F., Hanes, D.M., Kirby, J.T., Erikson, L.H., Barnard, P.L., 2011. Pressure-gradient-influenced nearshore circulations on an inlet-adjacent beach. Journal of Geophysical Research: Oceans. http://dx.doi.org/10.1029/2010JC006788.

Talke, S.A., Stacey, M.T., 2003. The influence of oceanic swell on flows over an estuarine intertidal mudflat in San Francisco Bay. Estuarine, Coastal, and Shelf Science 58 (3), 541–554.

Vincent, C.E., Hanes, D.M., 2002. The accumulation and decay of nearbed suspended sand concentration due to waves and wave groups. Continental Shelf Research 22 (14), 1987–2000.

Yu, X., Hsu, T.J., Hanes, D.M., 2010. Sediment transport under wave groups: relative importance between nonlinear wave shape and nonlinear boundary layer streaming. Journal of Geophysical Research: Oceans 115, C02013. http://dx.doi.org/10.1029/2009JC005348.